CHAPTER 11

Computational investigation on the molecular interactions of the p53(NTD)-RITA complex

Computational investigation on the molecular interactions of the p53(NTD)-RITA complex

11.1. Abstract:

An essential antagonistic regulator of the tumour suppressor p53 molecule is the protein MDM2. Therefore, it's crucial to restrict the binding between MDM2 and p53 molecules in order to regulate the p53 gene's activity. A small molecule RITA was identified as a p53 reactivating compound, causing the p53 molecules to resume their normal function. In this study, we have studied the structural dynamics and the interaction profile of p53(NTD)-RITA complex using molecular dynamics simulation. It was found that the molecule RITA innitially binds to the residues 33–37 of human p53. But throughout the course of the simulation, the small molecule RITA gets displaced and then gets bound to the TAD1 of p53(NTD). We also carried out the BFE as well as PRED analyses for the p53(NTD)-RITA complex. We found a good binding affinity between the TAD1 of p53(NTD) and RITA ($\Delta G_{binding}$ = -2.31 kcal mol^{-1}). The residues TRP23, GLU28, LEU26 and LEU14 of p53, which are present in the TAD1 of p53(NTD) provide the highest energy contributions for the interaction between p53(NTD) and RITA.

11.2. Introduction:

A protein known as p53, which has 393 amino acids, suppresses tumour growth. It also functions as a transcription factor, binding to certain DNA sequences to trans-activate a variety of genes in response to various genotoxic stresses. This can result in the cell cycle being stopped, damaged DNA being repaired, or apoptosis being induced, depending on the cell destiny. [651, 652]. By using X-ray crystallography, the structure of the core DNA-binding domain of p53 (residues 94–312) was determined. The tetramerization domain of the p53 protein (residues 323–356) was determined using both NMR and X-ray crystallography. [653-655]. Protein-Protein Interactions (PPI) and post-translational processes like phosphorylation, acetylation, and isomerization of prolyls are both used to control the trans-activity of p53 [656-661]. Through these processes, p53 can choose a specific group of target promoters by altering both its structural makeup and its propensity to bind to DNA sequences that include changes in the downstream genes. The mechanism underlying downstream gene selectivity as well

as the ensuing cell fate, however, are still unknown [662].

MDM2 is a recognised antagonistic p53 regulator. Primarily, MDM2 interacts with p53 through its N Terminal Domain (NTD). Between p53 and MDM2, there is a feedback loop that maintains their mutual control [663]. When DNA damage or any other stimulus activates p53, it speeds up the transcription of MDM2 mRNAs and proteins, which causes MDM2 to bind to p53, directly hindering p53 functioning by means of three key mechanisms. First, p53 is directly ubiquitinated by MDM2 (an E3 ligase), which causes the p53 molecules to be degraded by proteasomes. Second, MDM2's NTD interacts with p53's TAD1, preventing p53 from binding to its target DNA and preventing transcription. Thirdly, MDM2 speeds up the release of p53 molecules from the cell's nucleus [664-666], preventing them from interacting with the nuclear target DNA needed for transcription. [667-670]. It's noteworthy that in human malignancies, amplification of the MDM2 gene and mutations of the tumour protein 53 (TP53) are mutually exclusive [671]. The gene responsible for making p53 is called *TP53*.

RITA (reactivation of p53 and induction of tumour cell apoptosis), was given the name by Issaeva *et al*., in 2004 [735]. It is a small molecule inhibitor that prevents the interaction between p53 and MDM2 [736], and it both increases the amount of wild-type p53 and restores its function. [737, 738]. The antiproliferative effects of RITA were examined in the isogenic p53-lacking variant (null variant) HCT116 TP53−/− and the wild-type p53-expressing CRC cell line HCT116 (TP53+/+). Contrary to HCT116 TP53−/− cells, p53-regulated genes, including several oncogenes like MYC, were significantly downregulated in HCT116 TP53+/+ cells after RITA therapy, as well as an increase in the expression of genes related to apoptosis, such as NOXA, and p53 targets implicated in cell cycle arrest, such as the CDK inhibitor p21 [739, 740].

In the present study, we have investigated the conformational dynamics and stability, as well as the interaction profile at the molecular level of the p53(NTD)-RITA complex. We also carried out BFE and PRED analyses to infer the binding characteristics and identify hotspot residues across the interface of p53(NTD) in the p53(NTD)-RITA complex.

11.3. Materials & Methods:

11.3.1. Preparation of the p53(NTD)-RITA system:

The 3-D structure of p53 NTD, comprising of amino acid residues from 2-65, was modelled using I- TASSER server by submitting the amino acid (2-65 res) sequence. Five models were then obtained. The best structure was then viewed using the UCSF Chimera software v.1.13.1.

The 3-D structure of Reactivating p53 and Inducing Tumor Apoptosis (RITA) molecule (PubChem CID: 374536), was procured from the PubChem server in SDF file format and then PDB file format for the same was obtained using the open Babel online server. The small molecule RITA was then visualised using the ArgusLab visualization software v.4.0.1, followed by its energy optimization by the UFF (universal force field).

The PatchDock web server was then used to prepare the p53(NTD)-RITA complex. The best docked model was chosen based on section based on the principle mentioned in section **7.3.1**.

11.3.2. MD simulation of the p53(NTD)-RITA complex:

The MD simulation study on the p53(NTD)-RITA complex was then performed using the Assisted Model Building with Energy Refinement (AMBER) 14 software package, where ff99SB force field parameters were used for the protein part of the system, while the ligand (RITA) was treated with the generalized AMBER force field (GAFF) parameters. The rest of the steps were performed as mention in section **7.3.2**.

11.3.3. Analysis of the MD Trajectories:

The analysis of the MD trajectories have been performed using the modules mentioned in section **4.3.3**.

11.3.4. LigPlot Analysis of the p53(NTD)-RITA complex:

Using the RMSD clustering algorithm, the conformer of the complex at the beginning of the simulation (0 ns) and the conformer of the complex at the end of the simulation (50 ns) were extracted from the 50 ns MD trajectories. The confermers were then subjected to Ligplot analysis to obtain the Protein-Ligand interaction profiles.

11.3.5. BFE and PRED Analyses of the p53(NTD)-RITA complex:

The BFE and the PRED of the p53(NTD)-RITA complex interface residues analyses were calculated using the procedure mentioned in section **4.3.6.**

11.3.6. Determination of the interface residues:

Using the RMSD clustering algorithm, p53(NTD)-RITA complex stucture conformers at the beginning of the simulation (0 ns), as well as at the end of the simulation (50 ns) were extracted. Then RITA was removed from the both the conformers of the p53(NTD)-RITA complex. On the other hand the 3-D structure of MDM2 bound to the TAD1 of p53 protein (PDB ID: 1YCR) was obtained from the RCSB PDB [27], followed by the extraction of MDM2(NTD) from the p53-MDM2 complex. Then, the p53(NTD) extracted from the 0 ns connformer was docked with the MDM2(NTD) extracted (System 1), on the other hand, the p53(NTD) extracted from the 50 ns connformer was docked with the MDM2(NTD) extracted (System 2). using ClusPro 2.0 online server. Both the complex structures obtained (System 1 and 2) were then uploaded in the PDBsum server to obtain the Protein-Protein interaction profiles.

11.4. Results & Discussions:

11.4.1. Analysis of the conformational changes of the p53(NTD)-RITA Complex:

We have performed MD simulation on the p53(NTD)-RITA complex. After equilibration, the complex was subjected to production dynamics for 50 ns (**Figure 11.1**). From **Figure 11.1**, it can be observed that RITA, initially binds to the region 32-

36 residues of p53(NTD). But from 10 ns onwards, it was found to remain bound to the TAD1 of p53(NTD) throughout the simulation.

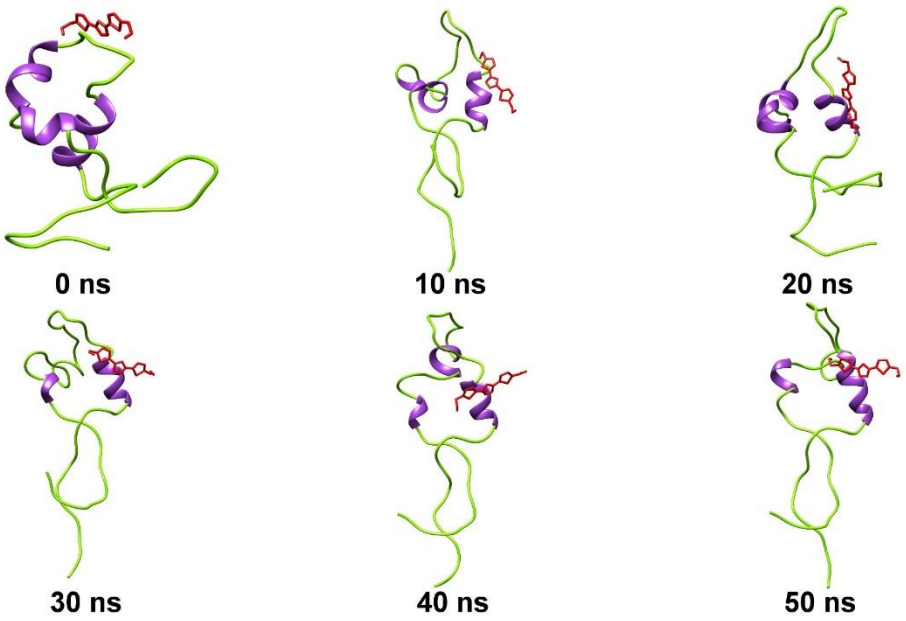

Figure 11.1. *Conformations of p53(NTD)-RITA at different time intervals of simulation.*

11.4.2. LigPlot Analysis of the various conformations of the p53(NTD)-RITA Complex:

The structures of the complex extracted at different intervals of MD simulation were then subjected to LigPlot analysis to obtain the protein ligand interaction profiles (**Figure 11.2**). It was found that initially the small molecule RITA binds to the residues 32-36 of p53(NTD). But in the 10 ns conformer, it can be observed that RITA gets displaced from the p53 residues 33-36, and then gets bound to the p53 TAD1 residues. It can also be observed that in 20, 30, 40, and 50 ns conformers also the small molecule RITA remains bound to the TAD1 of p53.

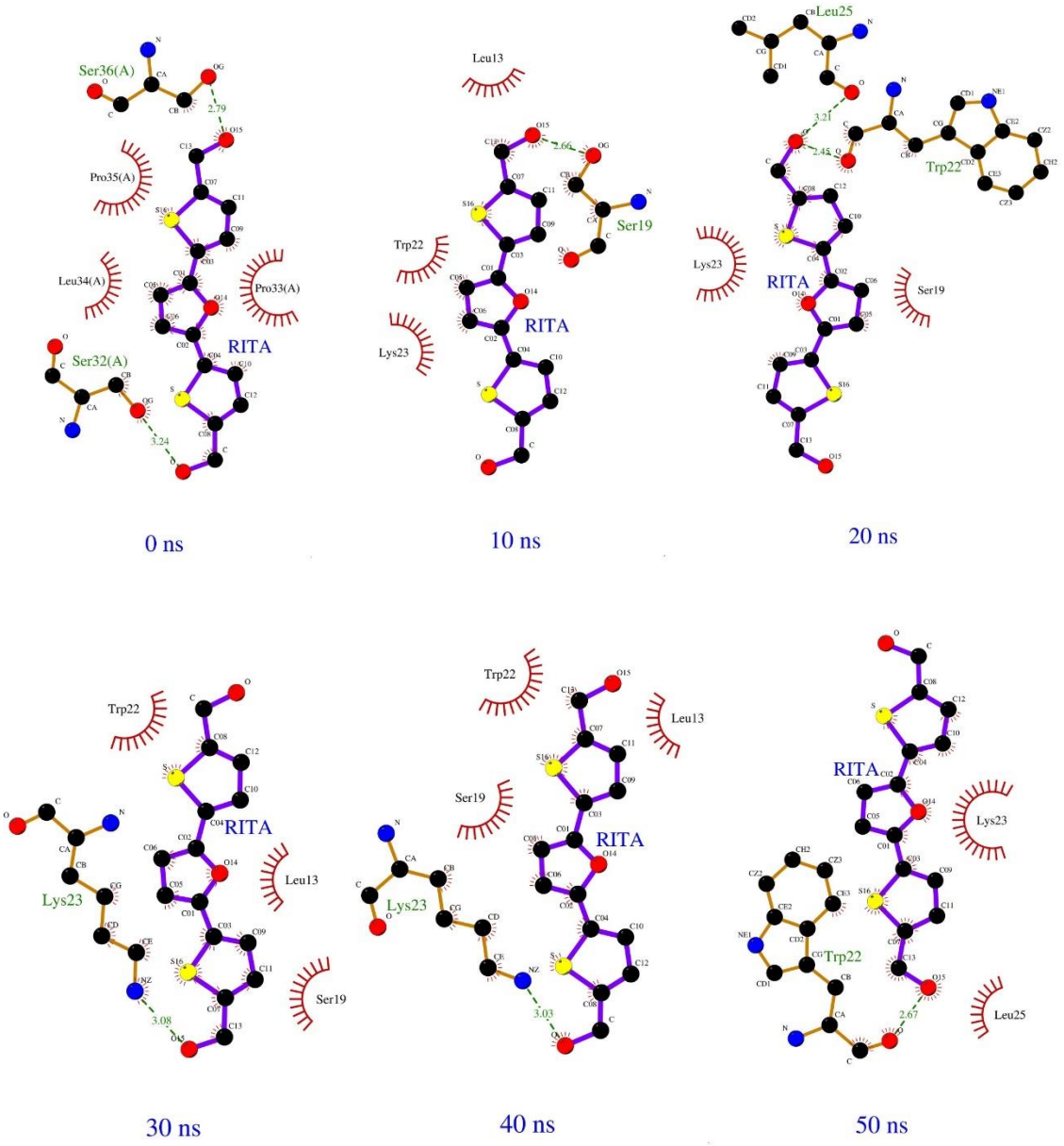

Figure 11.2. *LigPlot analysis of p53(NTD)-RITA at different time intervals of simulation.*

Various structural properties such as RMSD, RMSF, Rg, SASA, number of intermolecular hydrogen bonds, and the secondary structural elements were evaluated separately for p53(NTD)-RITA complex.

11.4.3. RMSD analysis of the p53(NTD)-RITA Complex:

The RMSD graph was plotted for Cα atoms for the complex as shown in **Figure 11.3**. We observed RMSD oscillate till 10 ns of simulation time and then found settled for the

rest of the simulation time. The average RMSD value of p53(NTD)-RITA complex was found to be 7.5 Å. The settling of the graph at 10 ns might indicate that during the simulation from 0 ns to 10 ns, RITA gets displaced from the p53 residues 32-36 and then gets bound firmly to the TAD1 of p53.

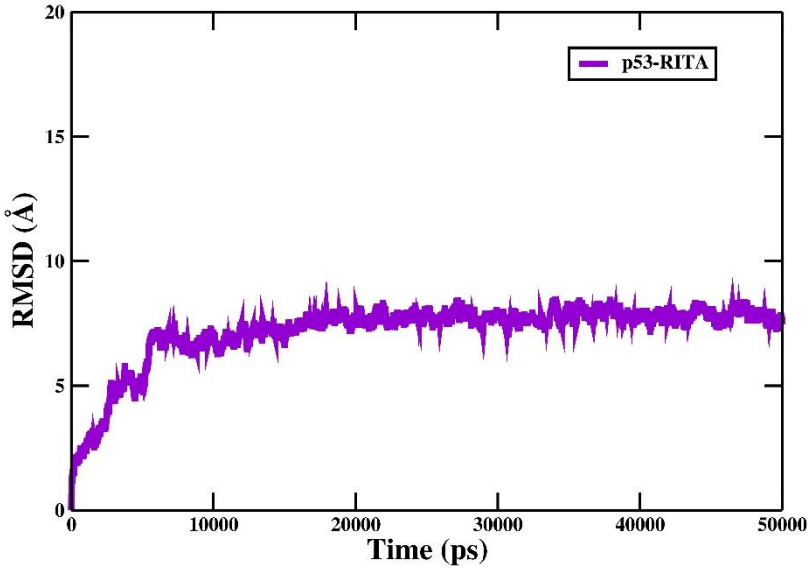

Figure 11.3. *RMSD analysis of p53(NTD)-RITA complex.*

11.4.4. RMSF analysis of the p53(NTD)-RITA Complex:

Then we determined the Residue flexibility in the p53(NTD)-RITA complex using RMSF analysis. **Figure 11.4.** shows the RMSF values for C-α atoms of the complex. From the RMSF plot, we see fluctuation of C-α atoms only in the N-Terminal and C-Terminal residues of p53(NTD).

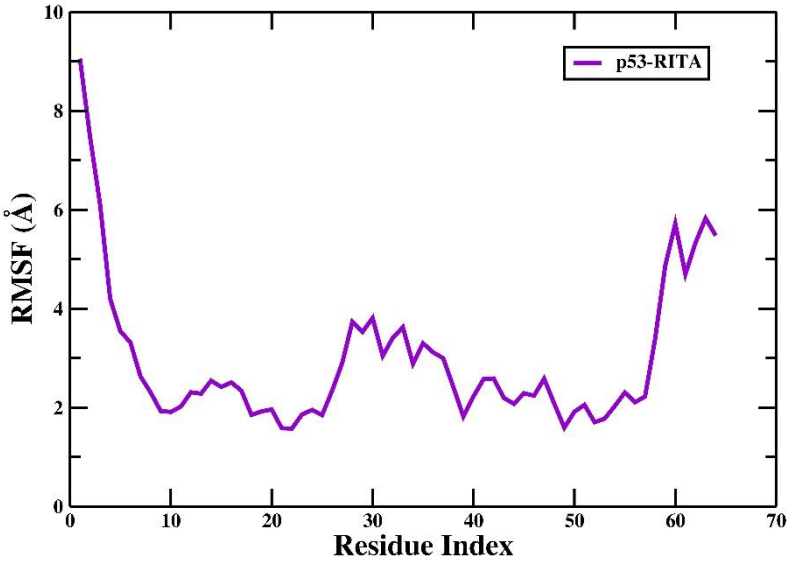

Figure 11.4. *RMSF analysis of p53(NTD)-RITA complex.*

11.4.5. Rg analysis of the p53(NTD)-RITA Complex:

Rg is another important geometrical parameter, which indicates the compactness of a system over a period of simulation time. A protein molecule must maintain its compactness at the right temperature and pressure to be considered stable. The average Rg values for the p53(NTD)-RITA complex was found to be 15 Å, which remained constant throughout the simulation (**Figure 11.5**).

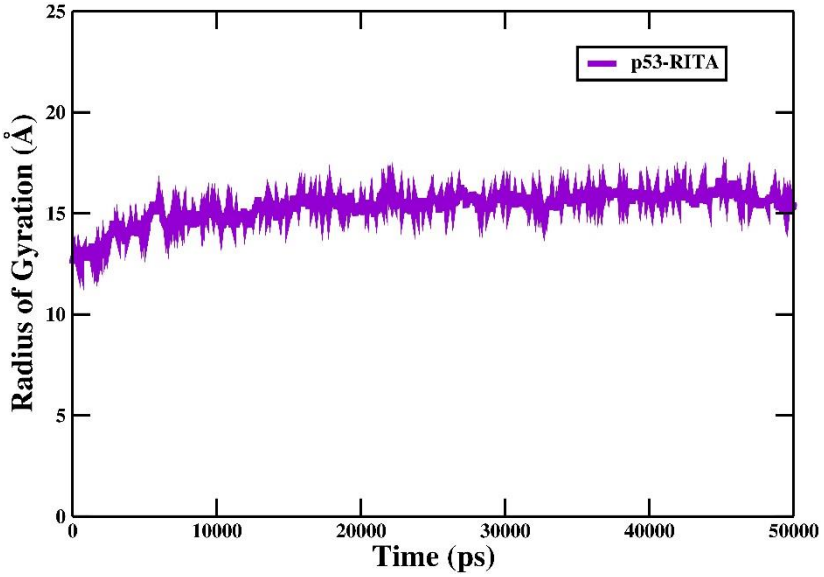

Figure 11.5. *Rg analysis of p53(NTD)-RITA complex.*

11.4.6. SASA analysis of the p53(NTD)-RITA Complex:

The SASA gives an overview of the behavior of residues with respect to solvent, and determines the stability of the protein. The SASA for p53(NTD)-RITA complex was calculated to be 6000 $Å^2$ (**Figure 11.6**).

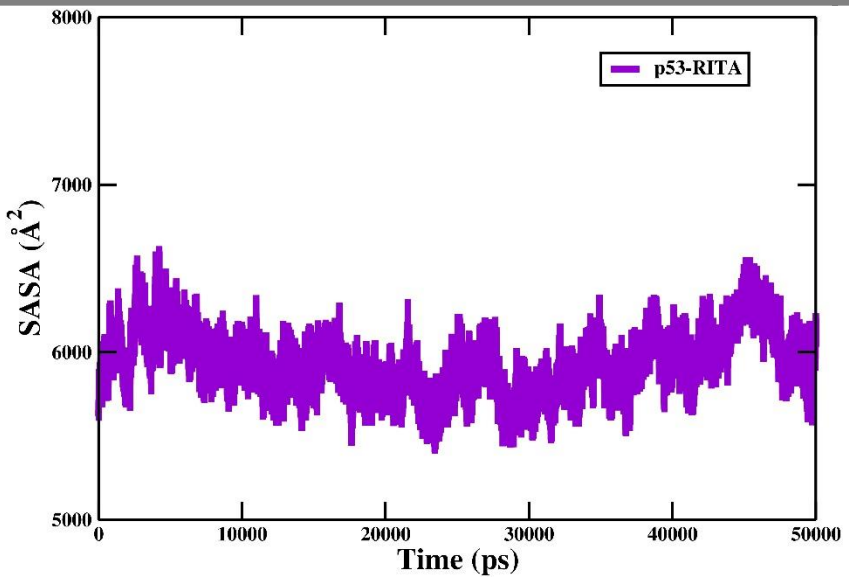

Figure 11.6. *SASA analysis of p53(NTD)-RITA complex.*

11.4.7. Hydrogen bond analysis of the p53(NTD)-RITA Complex:

Additionally, we also carried out the analysis of inter-molecular hydrogen bonds present in the p53(NTD)-RITA complex. The number of hydrogen bonds was observed to be within the ideal range as proposed for the globular proteins. **Figure 11.7** represents the intermolecular hydrogen bond analysis of the complex. The average number of intermolecular hydrogen bonds in the complex with p53(NTD) as donor and RITA as acceptor was found to be 1, and with RITA as donor and p53(NTD) as acceptor was found to be 4.

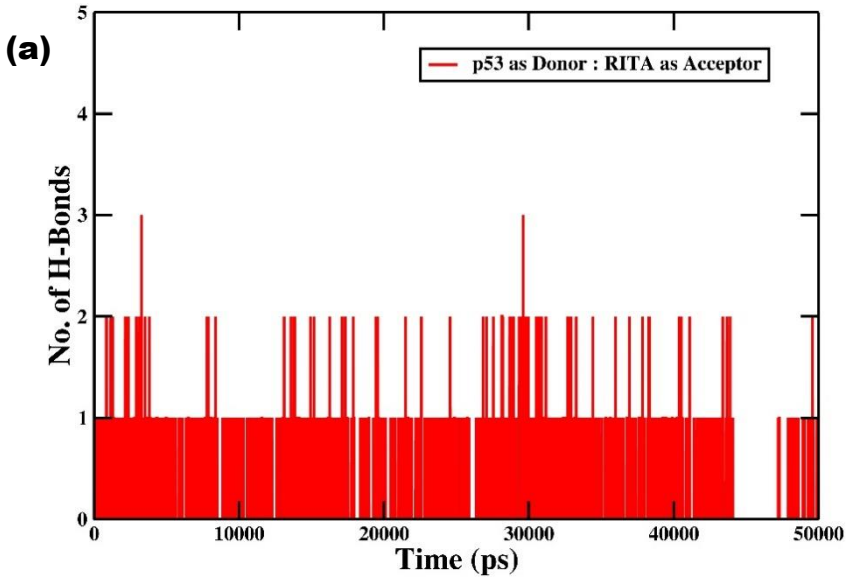

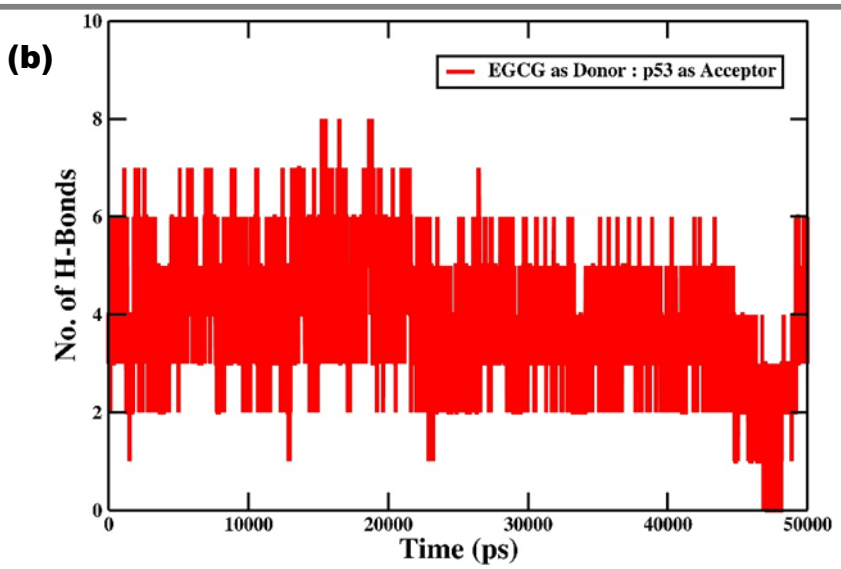

Figure 11.7. *Inter-molecular hydrogen bond analysis of p53(NTD)-RITA complex with (a) p53 as Donor and RITA as acceptor; and (b) RITA as Donor and p53 as acceptor.*

11.4.8. Analysis of probable secondary structure per residue of p53(NTD) in the p53(NTD)-RITA Complex:

Then we carried out the analysis of the probable secondary structure that each residue of p53(NTD) can adopt in p53(NTD)-RITA complex (**Figure 11.8**). From **Figure 11.8,** it can be observed that the p53(NTD) molecule contains the secondary structure α-helix predominantly in the regions 15-24, 34-42, and 44 -50 residues.

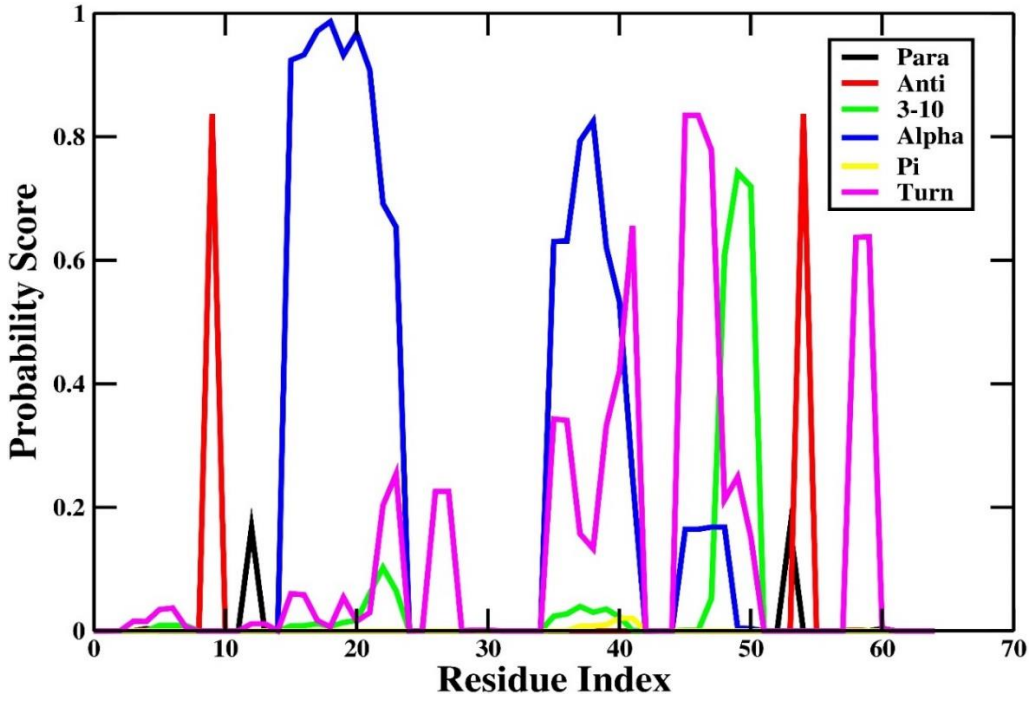

Figure 11.8. *Probability score for secondary structure analysis of p53(NTD) in the p53(NTD)-RITA complex.*

11.4.9. DSSP analysis of p53(NTD) in the p53(NTD)-RITA Complex:

Then we performed the DSSP analysis using the Kabsch and Sander algorithm to study the changes in secondary structural elements in the p53(NTD) molecule (as shown in **Figure 11.9**). From **Figure 11.9**, it can be observed that there is an increase in the α/310-helix content during the simulation, specifically in the residues: 16-25, 36-43, and 49-52, resulting in a good binding affinity between p53(NTD) and RITA.

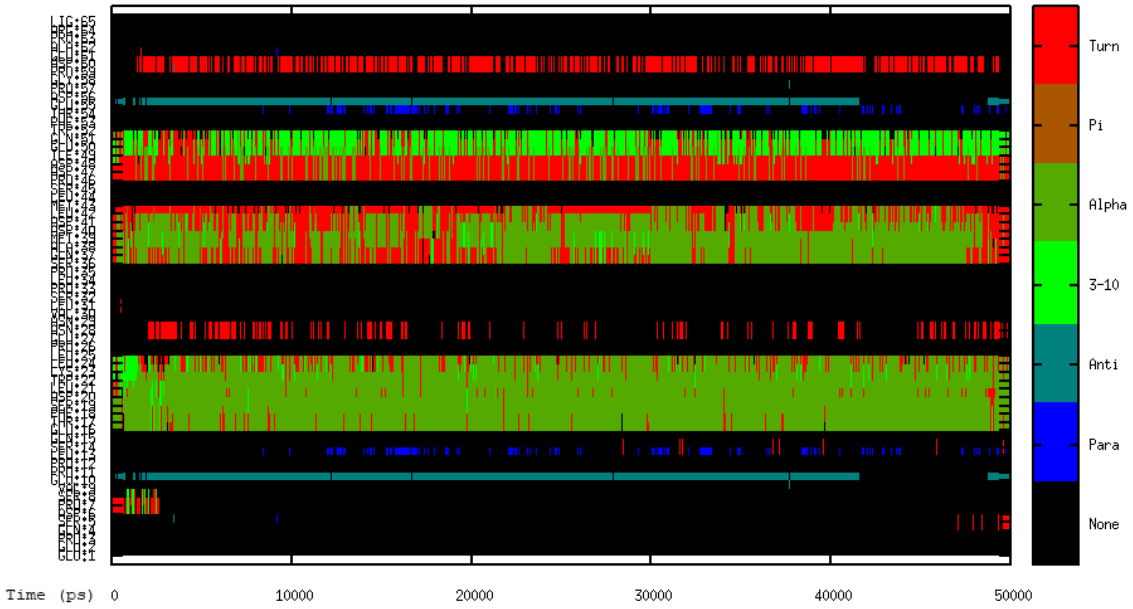

Figure 11.9. *DSSP analysis for p53(NTD) present in the p53-RITA complex. The secondary structure components are color-coded as shown in the panel.*

11.4.10. Secondary Structure analysis of the conformers of the p53(NTD)-RITA Complex:

Then, the secondary structure content of p53(NTD) present in the p53(NTD)-RITA complex at the beginning of the simulation (0 ns), as well as at the end of the simulation (50 ns) have been calculated using the 2StrucCompare server (**Table 11.1**), by extracting the conformers using RMSD clustering algorithm, and then uploading them in the online server. It was found that p53(NTD) in the p53(NTD)-RITA complex at 0 ns has 25.0% helices, while p53(NTD) in the p53(NTD)-RITA complex at 50 ns has 31.3% helices.

Table 11.1. *Secondary structure analysis of the initial and final structures of p53(NTD)-RITA complex using 2Struc online server.*

p53(NTD)-RITA	***α-Helix***	***3_{10}-Helix***	***Turns (%)***

	(%)	*(%)*	
0 ns	*25.0*	*0*	*7.8*
50 ns	*31.3*	*0*	*6.3*

11.4.11. BFE and PRED analyses of the p53(NTD)-RITA Complex:

The BFE calculations of p53(NTD) and RITA to form the p53(NTD)-RITA complex were performed using the MM-GBSA method, a module of the AMBER14 software package. The BFE evaluated for the p53(NTD)-RITA complex, together with the descriptions of the energy terms, are shown in **Table 11.2**. From **Table 11.2**, all the derived components required for the BFE analysis have been observed to contribute to the binding of p53(NTD) and RITA to form the p53(NTD)-RITA complex. The total BFE ($\Delta G_{binding}$) was found to be -2.31 kcal mol $^{-1}$, which indicates a good binding affinity between p53(NTD) and RITA molecule in the p53(NTD)-RITA complex.

Table 10.2. *The various components of the BFE (kcal mol^{-1}) evaluated by MM/GBSA method between p53(NTD)-RITA complex.*

Components	**Complex (kcal mol^{-1})**	**Standard Deviation (±)**	**Receptor (kcal mol^{-1})**	**Standard Deviation (±)**	**Ligand (kcal mol^{-1})**	**Standard Deviation (±)**	**$\Delta\Delta G_{bind}$ (kcal mol^{-1})**	**Standard Deviation (±)**
$\Delta E_{VDWAALS}$	-381.54	8.27	-360.28	7.93	-1.41	0.43	-19.85	1.82
ΔE_{EL}	-2849.09	26.77	-2838.12	26.42	-2.48	1.75	-8.49	4.15
ΔE_{GB}	-3181.81	23.10	-3177.37	22.81	-20.27	1.48	15.83	3.73
ΔE_{SURF}	42.84	0.58	42.49	0.56	3.01	0.02	-2.66	0.15
ΔG_{gas}	-3230.62	27.40	-3198.39	26.53	-3.89	1.77	-28.34	4.14
ΔG_{solv}	-3138.96	22.85	-3134.87	22.59	-17.27	1.48	13.18	3.70
ΔG_{TOTAL}	-6369.59	14.49	-6333.26	14.20	-21.15	2.14	**-15.17**	1.80
TS_{TRA}	15.67	0	15.63	0	12.79	0	-12.75	0
TS_{ROT}	15.70	0.01	15.65	0.01	10.27	0	-10.22	0
TS_{VIB}	757.55	2.95	727.71	3.12	19.73	0.57	10.11	2.10
TS_{TOTAL}	788.92	2.96	759.00	3.13	42.78	0.57	**-12.86**	2.11
$\Delta G_{binding}$							**-2.31**	

ΔE_{EL} = electrostatic energy as calculated by the MM force field; **$\Delta E_{VDWAALS}$** = van der Waals contribution from MM; **ΔE_{GB}** = the electrostatic contribution to the polar

solvation free energy calculated by GB; ΔE_{SURF} = non-polar contribution to the solvation free energy calculated by an empirical model; ΔG_{gas} = total gas phase energy ($\Delta G_{gas} = \Delta E_{EL} + \Delta E_{VDWAALS}$);$\Delta G_{solv}$ = sum of nonpolar and polar contributions to solvation; ΔG_{TOTAL} = final estimated binding free energy in kcal mol^{-1} calculated from the terms above ($\Delta G_{TOTAL} = \Delta G_{gas} + \Delta G_{solv}$); TS_{TRA} = translational energy; TS_{ROT} = rotational energy; TS_{VIB} = vibrational energy; TS_{TOTAL} = total entropic contribution; and $\Delta G_{binding}$ = BFE.

To have an insight into the influence of each of the amino acid residues of p53(NTD) on the overall p53(NTD)-RITA interaction, PRED values were determined implying the MM-GBSA method. **Figure 11.10** represents the PRED analysis for the interface residues of p53(NTD) present in the p53(NTD)-RITA complex. The highest energy contribution can be observed from the residue TRP23, followed by residues GLU28, LEU26 and LEU14 of p53 respectively, which are present in the TAD1 of p53(NTD).

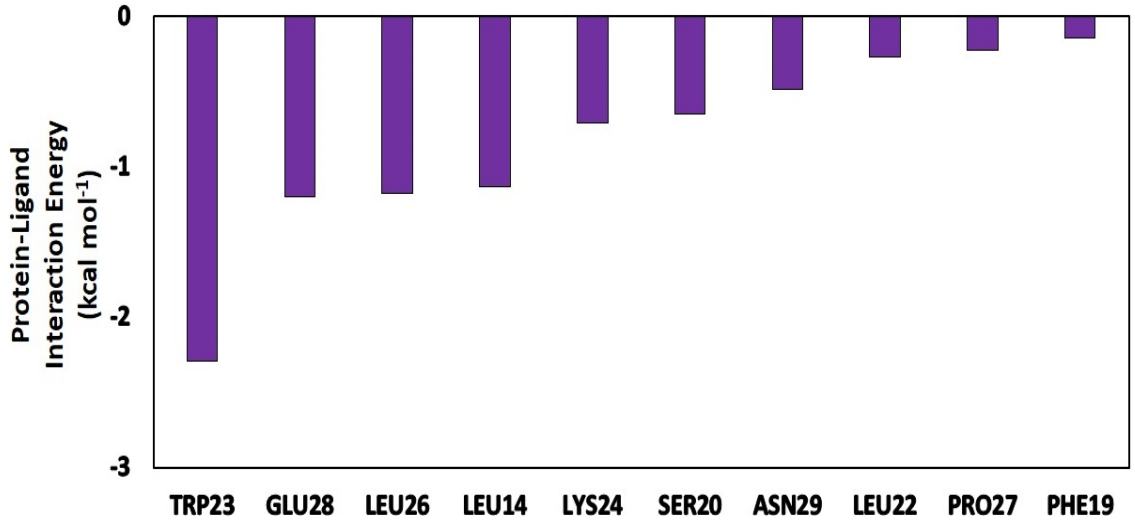

Figure 11.10. *Per Residue Energy Decomposition (PRED) analysis of p53(NTD) in p53(NTD)-RITA complex.*

11.4.12. Determination of the interface residues of the conformers of the p53(NTD)-RITA Complex:

Then, the two systems mentioned earlier: Sytem 1 and 2 were visualised using UCSF Chimera software v.1.13.1. It can be observed that the TAD1 present in p53(NTD) fits into the binding cavity of MDM2(NTD) before MD simulation of p53(NTD)-RITA complex (**Figure 11.11a**). Whereas, the TAD1 present in p53(NTD) does not fit into the binding cavity of MDM2(NTD) at the end of MD simulation of p53(NTD)-RITA complex (**Figure 11.11b**). This indicates that the p53(NTD), in complex with RITA,

undergoes conformational changes throughout the simulation, resulting in the disruption of p53(TAD1)-MDM2(NTD) interaction. Also, the total number of residues from MDM2(NTD) interacting p53(NTD) in system 1 is more than the total number of residues from MDM2(NTD) interacting p53(NTD) in system 2.

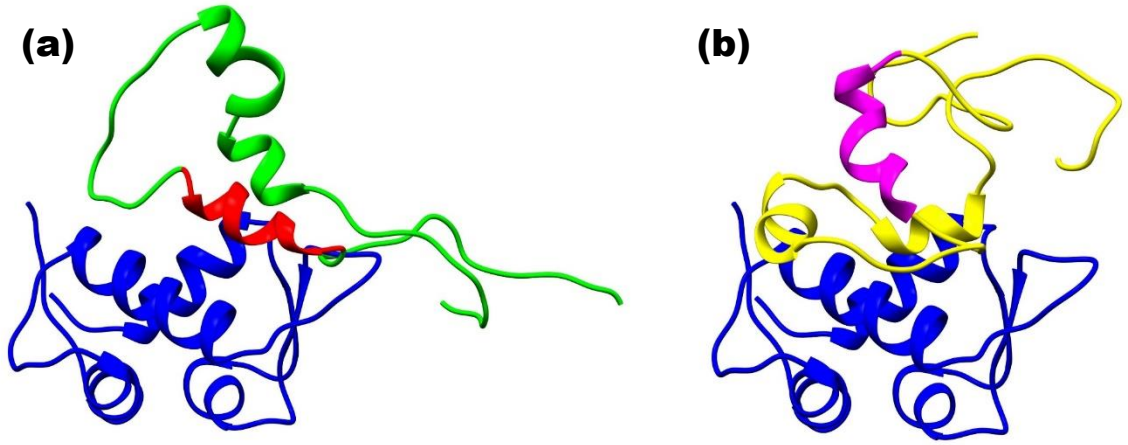

Figure 11.11. *MDM2(NTD) docked with p53(NTD) extracted from the p53(NTD)-RITA complex (a) before the MD simulation of the p53(NTD)-RITA complex, and (b) at the end of the MD simulation of the p53(NTD)-RITA complex. Blue=MDM2(NTD), Green=p53(NTD) before simulation, Red=p53(TAD1) before simulation, Yellow=p53(NTD) after simulation, Purple=p53(TAD1) after simulation.*

After obtaining the protein-protein interaction profiles of the two systems, they were compared with the protein-protein interaction profile of p53(TAD1)-MDM2(NTD), which is already present in the PDBsum Database (System 3). It can be observed that the number of residues from p53(NTD) interacting with MDM2(NTD) before simulation are more in common with p53(NTD) interacting with MDM2(NTD) in system 3 than the number of residues from p53(NTD) interacting with MDM2(NTD) at the end of simulation common with p53(NTD) interacting with MDM2(NTD) in system 3 (**Figure11.12**).

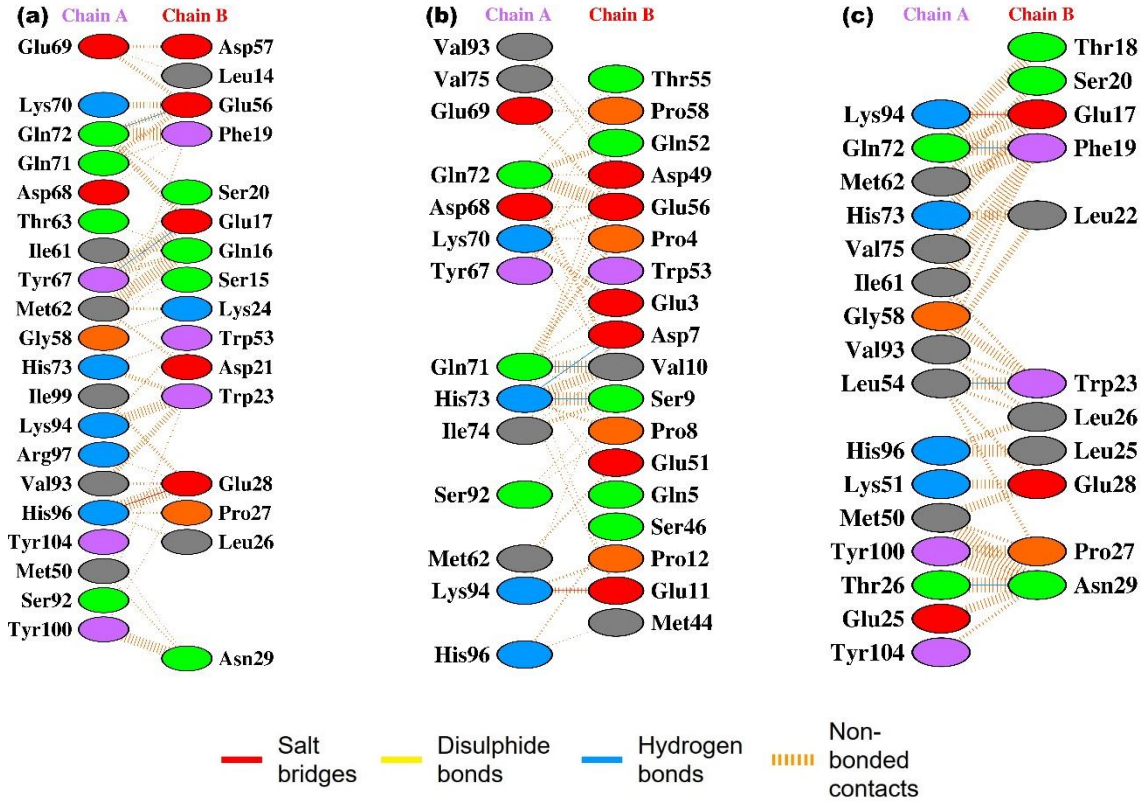

Figure 11.12. *Protein-Protein Interaction Profile of (a) MDM2(NTD)-p53(NTD) complex before p53-RITA simulation, (b) MDM2(NTD)-p53(NTD) complex after p53-RITA simulation, and (c) MDM2-p53 complex (PDB ID: 1YCR). Chain A: MDM2, Chain B: p53.*

11.5. Conclusion:

In this study, we have demonstrated the molecular interactions between p53(NTD) and its inhibitor RITA. The small molecule RITA initially binds to the residues 32-36 of p53(NTD). But throughout the course of simulation, RITA gets displaced (0 ns – 10 ns), and then gets bound to the TAD1 of p53(NTD (10 ns – 50 ns). There exists a good binding affinity between the p53(NTD) and RITA was ($\Delta G_{binding}$ = -2.31 kcal mol^{-1}). The residues TRP23, followed by residues GLU28, LEU26 and LEU14 of p53 respectively, provide the energy contribution for the interaction, which are present in the TAD1 of p53(NTD). Our study's findings might be applied to the development of stronger p53-MDM2 interaction inhibitors, improving the effectiveness of cancer therapy.